Electronic Supplementary Material (ESI) for Catalysis Science & Technology.

Supporting Information for

Selective Catalytic Reduction of NO with NH_3 over Cu-Exchanged CHA, GME, and AFX Zeolites: A Density Functional Theory Study

Pei Zhao,[a,b*] Bundet Boekfa,[c] Ken-ichi Shimizu,[b,d] Masaru Ogura,[b,e] and Masahiro Ehara[a,b*]

[a]*Research Center for Computational Science, Institute for Molecular Science, Okazaki, 444-8585, Japan.*

[b] *Element Strategy Initiative for Catalysts and Batteries (ESICB), Kyoto University, Kyoto 615-8245, Japan.*

[c]*Department of Chemistry, Faculty of Liberal Arts and Science, Kasetsart University, Kamphaengsaen Campus, Nakhonpathom 73140, Thailand.*

[d]*Institute for Catalysis, Hokkaido University, Sapporo 001-0021, Japan*

[e]*Institute of Industrial Science, The University of Tokyo, Tokyo 153-8505, Japan*

Contents

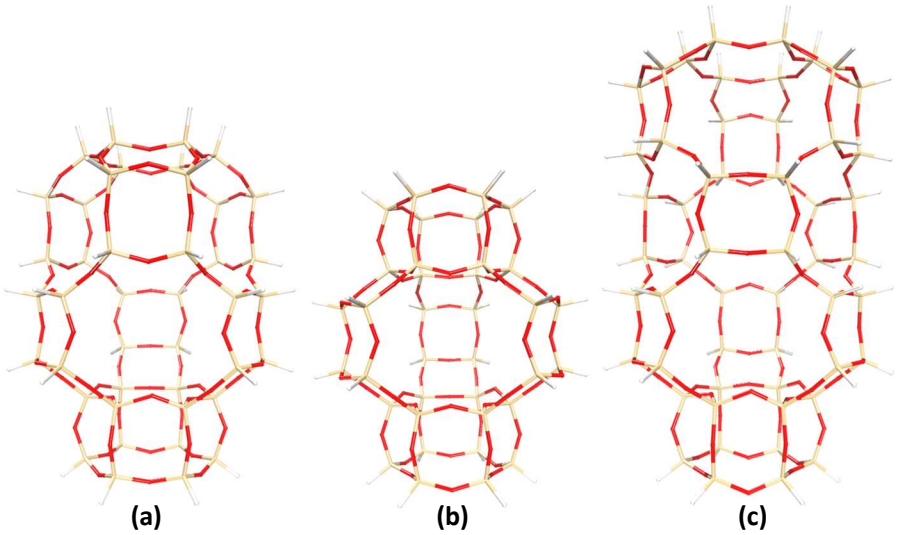

I. **Figure S1**. The computational models of *cha* (42T, a), *gme* (36T, b) and *aft* (54T, c). (Color code: Si tan; O red; H white.)

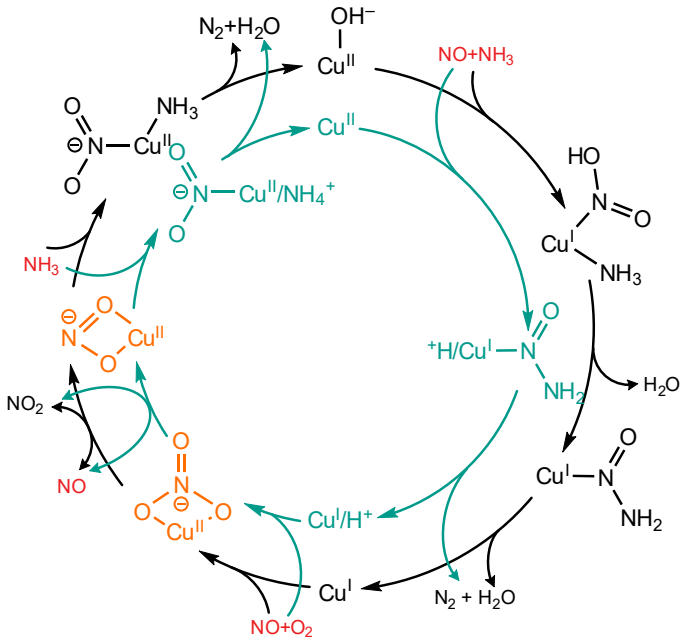

II. **Scheme S1.** The reaction mechanism for the SCR reaction in the Cu-zeolite. The reaction pathways for the oxidation of Cu^{I} and the reduction of Cu^{II} with one Al atom in the framework cages are represented in black (adapted from Janssens et al.[13]), while that with two Al atoms in the frameworks are represented in green (adapted from Schneider et al.[12]). The same intermediates on 1Al and 2Al sites are indicated in orange. Reactants and products are colored in red and black, respectively.

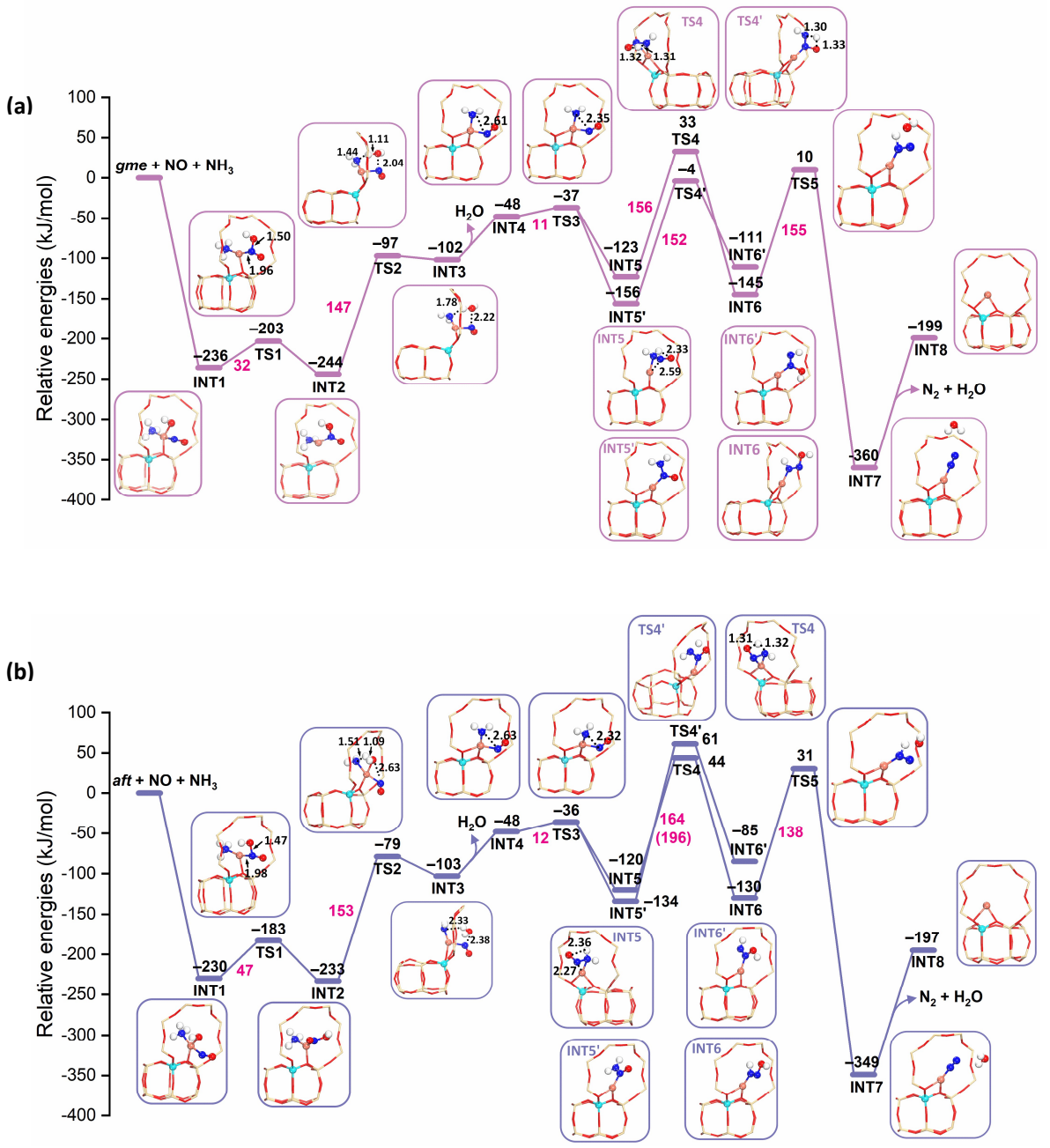

III. Figure S2. Reaction energy diagrams and optimized structures of intermediates and transition states for reduction by NO and NH_3 on $Cu^{II}OH$-Al-*gme* (a) and -*aft* (b). Values of reaction energies and energy barriers are shown in black and magenta, respectively. (The value in parenthesis for *aft* is the energy barrier between INT5' and INT6'.)

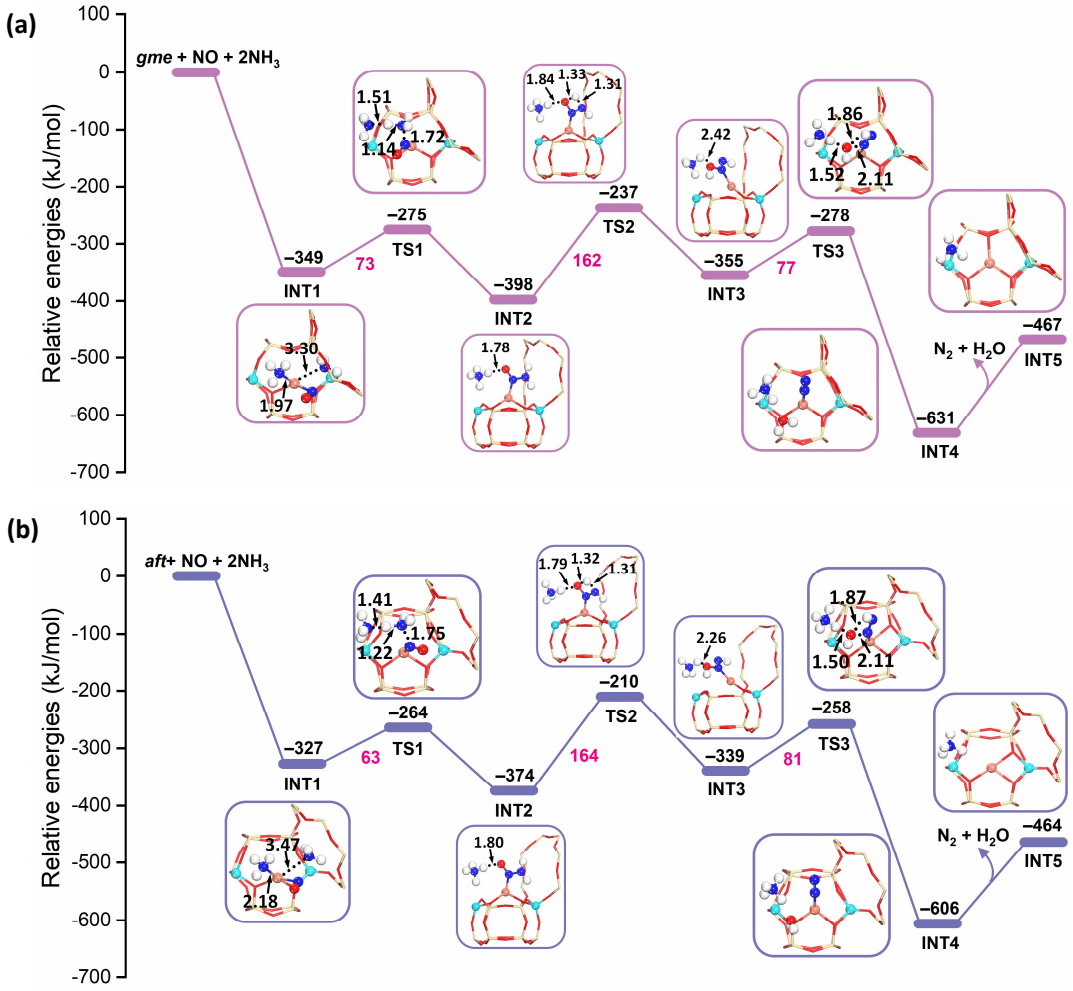

IV. Figure S3. Reaction energy diagrams and optimized structures of intermediates and transition states for reduction by NO and NH_3 on Cu^{II}-2Al-*gme* (a) and -*aft* (b).

V. Table S1. Deformation energies (kJ/mol) of intermediates and transition states with respect to the pristine structures of Cu^{II}-2Al-*cha*, -*gme*, and -*aft*.

Cage	INT1	TS1	INT2
cha	511	390	524
gme	520	412	547
aft	498	395	474

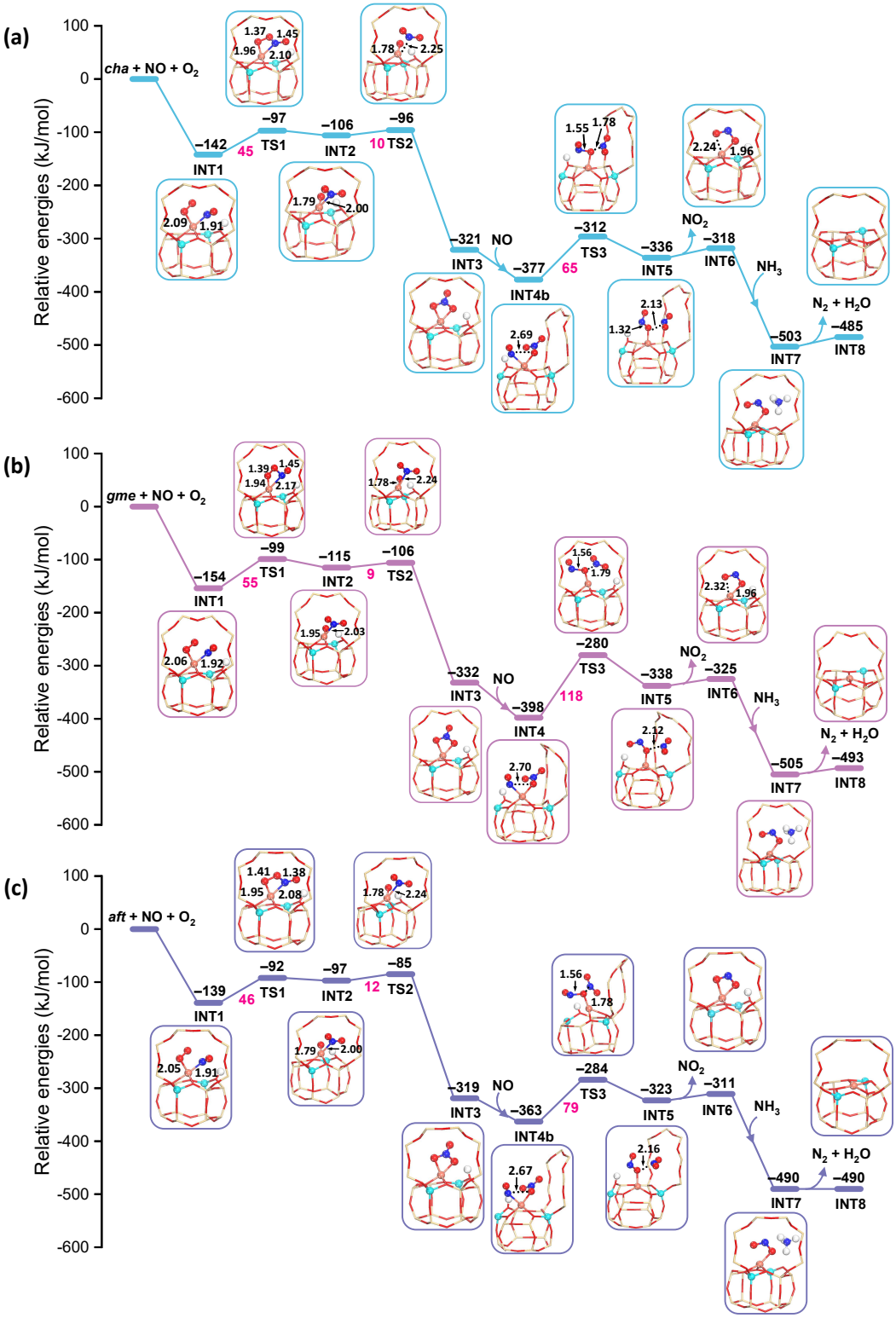

VI. **Figure S4**. Reaction energy diagrams and local structures of intermediates and transition states for oxidation by Cu^{I}-2AlH-*cha* (a), -*gme* (b), and -*aft*(c). Values of reaction energies and energy barriers are shown in black and magenta, respectively.

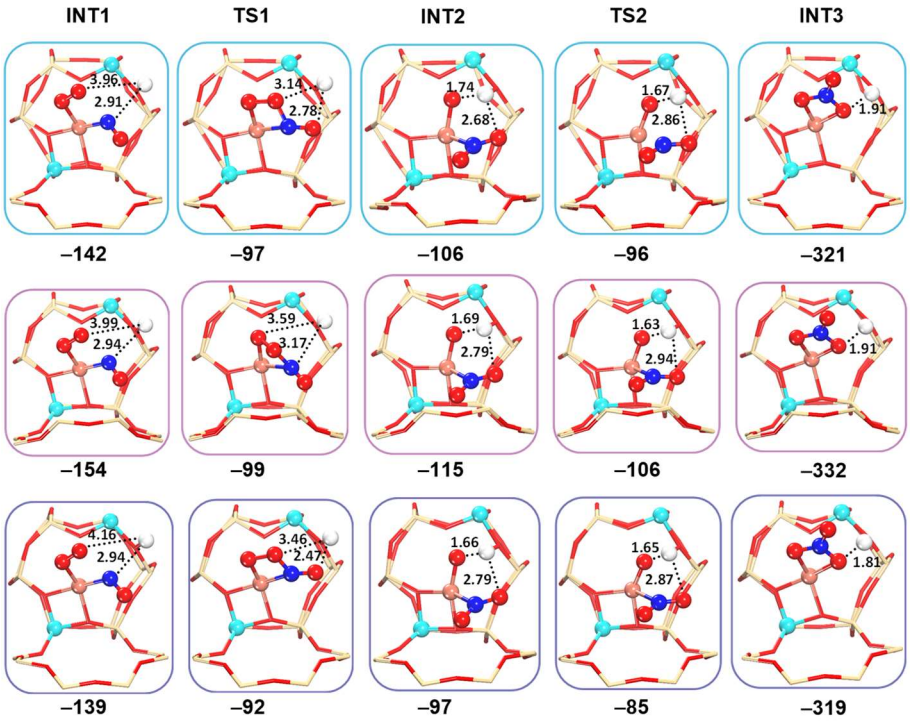

VII. **Figure S5.** Local geometries of the INT1, TS1, INT2, TS2 and INT3 of *cha* (blue), *gme* (pink), –and *aft* (purple) at the 2Al site. The distances between the adsorbed molecules and the Brønsted proton are shown in angstrom. The values beneath each structure are adsorption energies or reaction energies with respect to the isolated reactants.

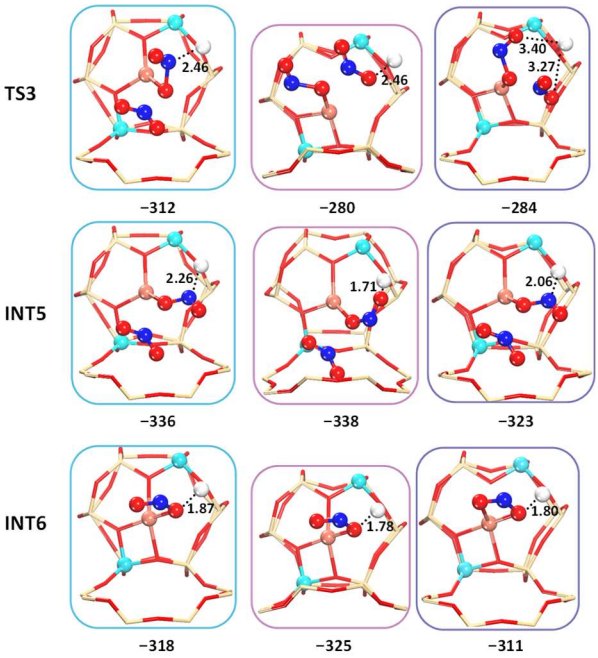

VIII. Figure S6. Local geometries of the TS3, INT5, and INT6 of *cha* (blue), *gme* (pink), and *aft* (purple) at the Al site. The distances between the adsorbed molecules and the Brønsted proton are shown in angstrom. The values beneath each structure are reaction energies with respect to the isolated reactants.

IX. Table S2. Deformation energies (kJ/mol) of intermediates and transition states for the oxidation with respect to the pristine structures of Cu^{I}-Al-*cha*, -*gme*, and -*aft*.

Cages	INT1	TS1	INT2	TS2	INT3	INT4	TS3	INT5	INT6	INT7
CHA	83	86	91	90	92	93	74	72	90	91
GME	85	90	95	92	93	98	89	67	88	88
AFT	73	79	86	83	84	84	72	74	83	87

X. Table S3. Deformation energies (kJ/mol) of intermediates and transition states for the oxidation with respect to the pristine structures of Cu^{I}-2AlH-*cha*, -*gme*, and -*aft*.

Cages	INT1	TS1	INT2	TS2
cha	77	83	147	136
gme	84	89	150	144
aft	83	90	163	148

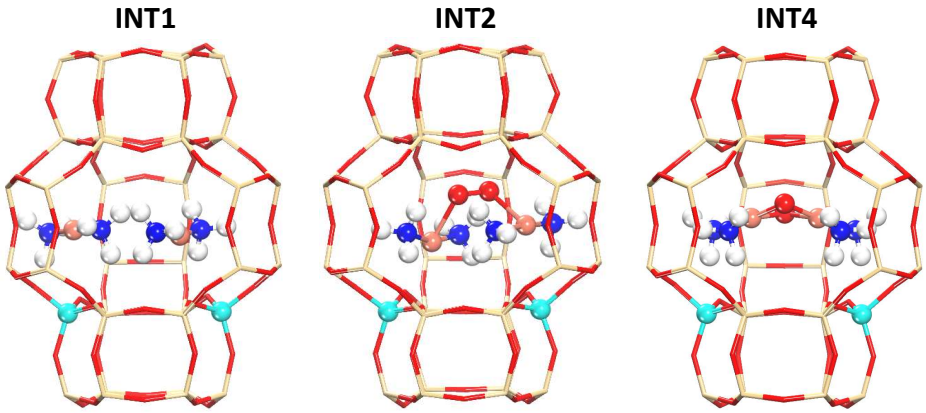

XI. **Figure S7.** Optimized structures and relative energies (kJ/mol) of INT1, INT2, and INT4 for the *gme* cage. The energies of INT2 and INT4 are obtained with respect to INT1 and O_2.

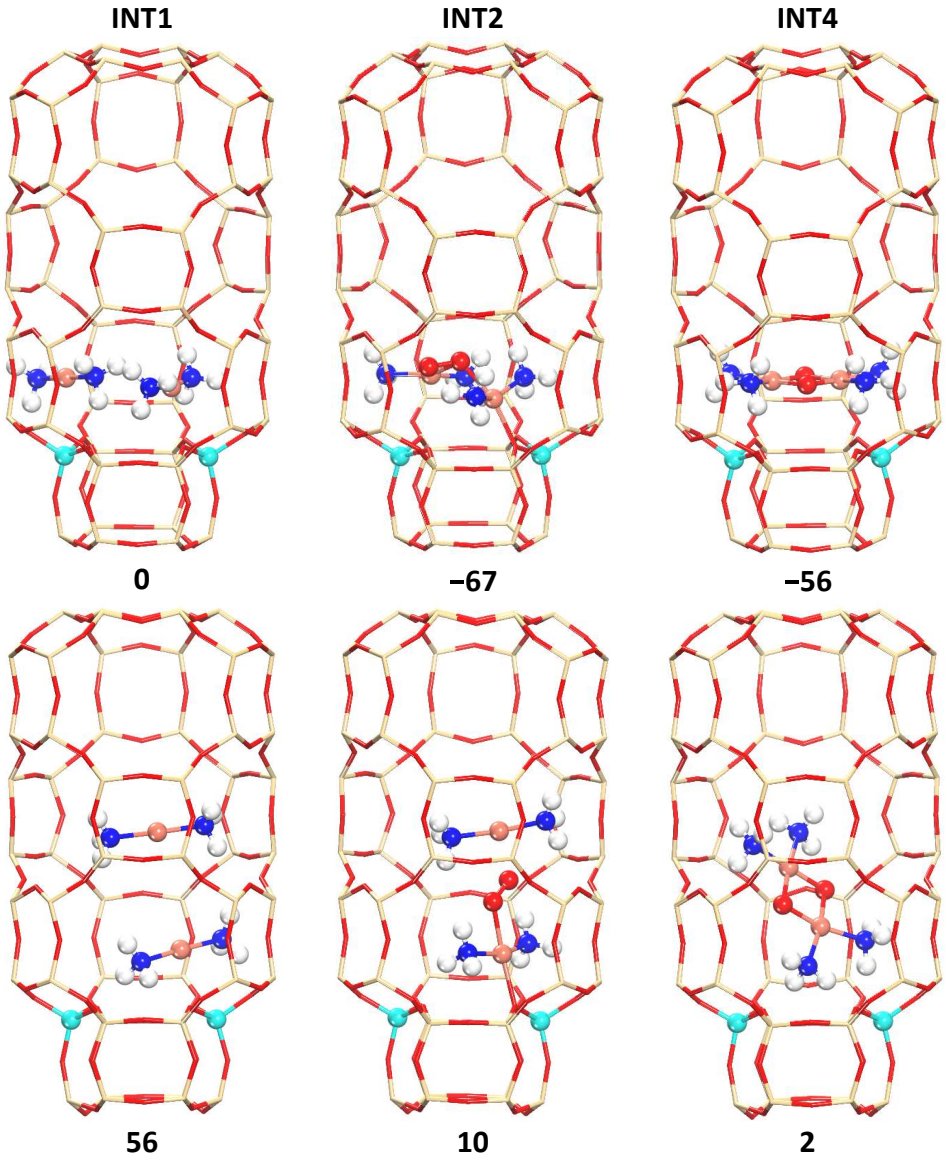

XII. Figure S8. Optimized structures and relative energies (kJ/mol) of INT1, INT2, and INT4 for the *aft* cage (top: para-site; bottom: per-site). The energies of INT2 and INT4 are obtained with respect to the para-site INT1 and O_2.

XIII. Table S4. Interaction energies (ΔE_{int}, in kJ/mol) between the $[zeolite]^{2-}$ cage and the inner $2[Cu^{I}(NH_3)_2]^{+}/2[OCu^{I}(NH_3)_2]^{+}$ ion in INT1 and INT4 as well as relative energies of the outer cage (ΔE_{cage}) and the inner species (ΔE_{Cu}) for *cha* and *aft*.

		INT1			INT4		
		ΔE_{int}	ΔE_{cage}	ΔE_{Cu}	ΔE_{int}	ΔE_{cage}	ΔE_{Cu}
cha	para	−1068	11	68	−1118	12	50
	per	−937	0	0	−1015	0	0
aft	para	−976	11	49	−1037	16	56
	per	−860	0	0	−908	0	0
gme	para	−1141	/	/	−1212	/	/

$\Delta E_{int} = E_{INT/TS}-(E_{cage} + E_{Cu})$
E_{cage} and E_{Cu} are single point energies of the outer cage and the inner species of INT/TS.

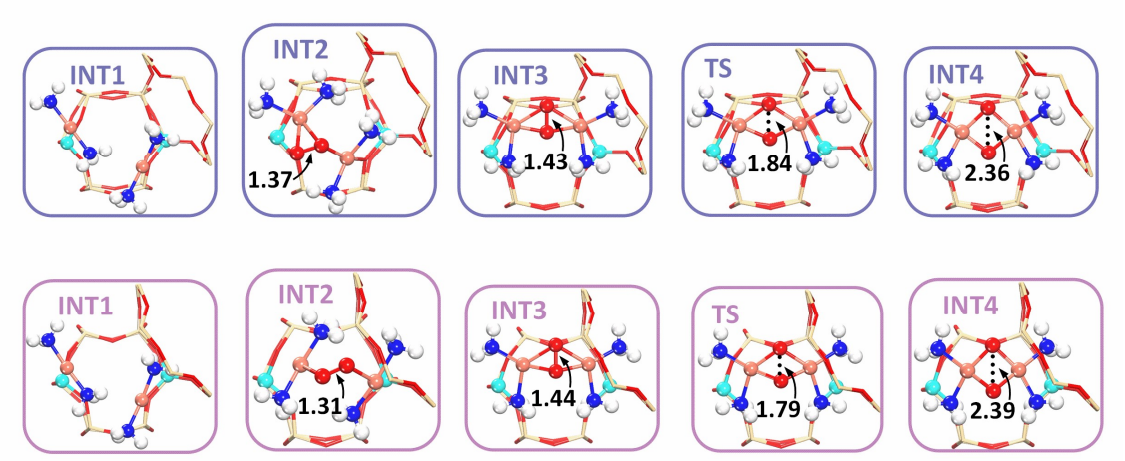

XIV. Figure S9. Local geometries of intermediates and transition states for the O_2 activation by the $2[NH_3\text{-}Cu^{I}\text{-}NH_3]$ dimer in 2Al -*gme* (pink), and -*aft* (purple).

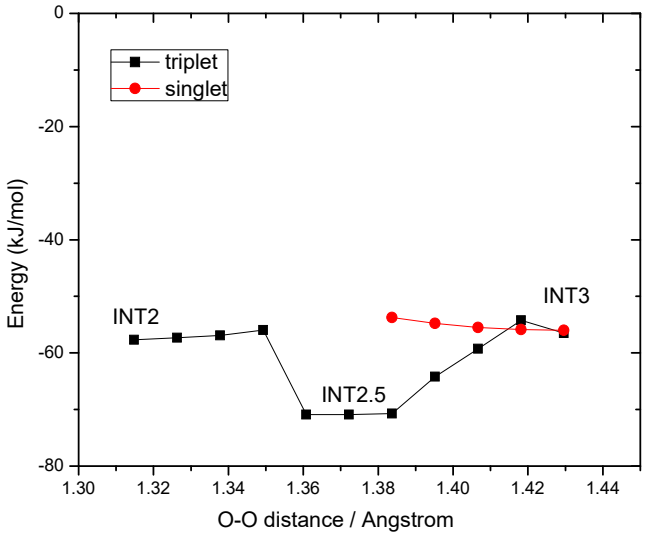

XV. **Figure S10.** Potential energy surface between INT2 and INT3 for the O_2 activation by the 2[NH_3-Cu^I-NH_3] dimer in 2Al-*cha*. Partial optimization was conducted with O-O distance being fixed and all the other coordinates optimized.

XVI. Natural electron configurations of Cu in Cu-*cha*, Cu-*gme*, and Cu-*aft*.

Table S5. Natural electron configurations of Cu in intermediates and transition states at the Al-$Cu^{II}OH$ site of Cu-*cha*, Cu-*gme*, and Cu-*aft*.

species	*cha*	*gme*	*aft*
Al-$Cu^{II}OH$	$4s^{0.38}3d^{9.36}4p^{0.23}4d^{0.01}$	$4s^{0.38}3d^{9.37}4p^{0.22}4d^{0.01}$	$4s^{0.39}3d^{9.36}4p^{0.22}4d^{0.01}$
INT1	$4s^{0.33}3d^{9.53}4p^{0.30}4d^{0.02}5p^{0.01}$	$4s^{0.34}3d^{9.53}4p^{0.28}4d^{0.02}5p^{0.01}$	$4s^{0.33}3d^{9.50}4p^{0.31}4d^{0.02}5p^{0.01}$
TS1	$4s^{0.31}3d^{9.72}4p^{0.24}4d^{0.02}5p^{0.01}$	$4s^{0.29}3d^{9.70}4p^{0.26}4d^{0.02}5p^{0.01}$	$4s^{0.32}3d^{9.72}4p^{0.24}4d^{0.02}5p^{0.01}$
INT2	$4s^{0.36}3d^{9.69}4p^{0.26}4d^{0.02}5p^{0.01}$	$4s^{0.35}3d^{9.70}4p^{0.25}4d^{0.02}5p^{0.01}$	$4s^{0.33}3d^{9.64}4p^{0.25}4d^{0.02}5p^{0.01}$
TS2	$4s^{0.35}3d^{9.49}4p^{0.34}4d^{0.01}$	$4s^{0.40}3d^{9.54}4p^{0.26}4d^{0.02}$	$4s^{0.33}3d^{9.41}4p^{0.40}4d^{0.02}5p^{0.01}$
INT3	$4s^{0.40}3d^{9.46}4p^{0.36}4d^{0.01}$	$4s^{0.40}3d^{9.50}4p^{0.29}4d^{0.01}5p^{0.01}$	$4s^{0.44}3d^{9.48}4p^{0.29}4d^{0.02}$
INT4	$4s^{0.38}3d^{9.43}4p^{0.37}4d^{0.01}$	$4s^{0.39}3d^{9.43}4p^{0.36}4d^{0.01}$	$4s^{0.39}3d^{9.41}4p^{0.36}4d^{0.01}$
TS3	$4s^{0.38}3d^{9.46}4p^{0.32}4d^{0.01}$	$4s^{0.38}3d^{9.47}4p^{0.33}4d^{0.01}$	$4s^{0.38}3d^{9.46}4p^{0.31}4d^{0.01}$
INT5	$4s^{0.37}3d^{9.71}4p^{0.18}4d^{0.01}$	$4s^{0.38}3d^{9.75}4p^{0.13}4d^{0.01}5p^{0.01}$	$4s^{0.32}3d^{9.70}4p^{0.18}4d^{0.01}$
TS4	$4s^{0.35}3d^{9.70}4p^{0.19}4d^{0.01}$	$4s^{0.30}3d^{9.61}4p^{0.21}4d^{0.01}$	$4s^{0.30}3d^{9.61}4p^{0.21}4d^{0.01}$
INT6	$4s^{0.33}3d^{9.68}4p^{0.20}5p^{0.01}$	$4s^{0.37}3d^{9.72}4p^{0.13}4d^{0.01}5p^{0.01}$	$4s^{0.36}3d^{9.71}4p^{0.14}4d^{0.01}$
TS5	$4s^{0.32}3d^{9.69}4p^{0.18}4d^{0.01}$	$4s^{0.33}3d^{9.70}4p^{0.15}4d^{0.01}5p^{0.01}$	$4s^{0.32}3d^{9.68}4p^{0.17}4d^{0.01}$
INT7	$4s^{0.27}3d^{9.73}4p^{0.30}4d^{0.01}$	$4s^{0.33}3d^{9.68}4p^{0.20}$	$4s^{0.33}3d^{9.66}4p^{0.21}$
INT8	$4s^{0.18}3d^{9.93}4p^{0.07}5p^{0.01}$	$4s^{0.19}3d^{9.92}4p^{0.07}5p^{0.01}$	$4s^{0.20}3d^{9.92}4p^{0.07}5p^{0.01}$

Table S6. Natural electron configurations of Cu in intermediates and transition states at the 2Al-Cu^{II} site of Cu-*cha*, Cu-*gme*, and Cu-*aft*.

species	*cha*	*gme*	*aft*
2Al-Cu^{II}	$4s^{0.29}3d^{9.30}4p^{0.21}4d^{0.01}5p^{0.01}$	$4s^{0.29}3d^{9.30}4p^{0.22}4d^{0.01}5p^{0.01}$	$4s^{0.30}3d^{9.30}4p^{0.23}4d^{0.01}5p^{0.01}$
INT1	$4s^{0.34}3d^{9.52}4p^{0.26}4d^{0.02}5p^{0.01}$	$4s^{0.33}3d^{9.51}4p^{0.27}4d^{0.02}5p^{0.01}$	$4s^{0.34}3d^{9.52}4p^{0.26}4d^{0.02}5p^{0.01}$
TS1	$4s^{0.27}3d^{9.60}4p^{0.26}4d^{0.02}5p^{0.01}$	$4s^{0.24}3d^{9.59}4p^{0.29}4d^{0.02}5p^{0.01}$	$4s^{0.24}3d^{9.62}4p^{0.28}4d^{0.02}5p^{0.01}$
INT2	$4s^{0.29}3d^{9.76}4p^{0.22}4d^{0.02}5p^{0.01}$	$4s^{0.28}3d^{9.76}4p^{0.23}4d^{0.02}5p^{0.01}$	$4s^{0.30}3d^{9.76}4p^{0.21}4d^{0.02}5p^{0.01}$
TS2	$4s^{0.28}3d^{9.73}4p^{0.21}4d^{0.02}5p^{0.01}$	$4s^{0.27}3d^{9.72}4p^{0.24}4d^{0.02}5p^{0.01}$	$4s^{0.26}3d^{9.74}4p^{0.21}4d^{0.02}5p^{0.01}$
INT3	$4s^{0.39}3d^{9.73}4p^{0.19}4d^{0.01}5p^{0.01}$	$4s^{0.34}3d^{9.73}4p^{0.22}4d^{0.02}5p^{0.01}$	$4s^{0.37}3d^{9.73}4p^{0.19}4d^{0.01}5p^{0.01}$
TS3	$4s^{0.25}3d^{9.60}4p^{0.26}4d^{0.02}5p^{0.01}$	$4s^{0.25}3d^{9.59}4p^{0.28}4d^{0.01}5p^{0.01}$	$4s^{0.24}3d^{9.60}4p^{0.27}4d^{0.02}5p^{0.01}$
INT4	$4s^{0.28}3d^{9.73}4p^{0.25}4d^{0.02}5p^{0.01}$	$4s^{0.27}3d^{9.71}4p^{0.27}4d^{0.02}5p^{0.01}$	$4s^{0.25}3d^{9.76}4p^{0.26}4d^{0.02}5p^{0.01}$
INT5	$4s^{0.33}3d^{9.84}4p^{0.17}4d^{0.01}5p^{0.01}$	$4s^{0.27}3d^{9.87}4p^{0.19}4d^{0.01}5p^{0.01}$	$4s^{0.32}3d^{9.85}4p^{0.17}4d^{0.01}5p^{0.01}$

Table S7. Natural electron configurations of Cu in intermediates and transition states at the Al-Cu^{I} site of Cu-*cha*, Cu-*gme*, and Cu-*aft*.

species	*cha*	*gme*	*aft*
Al-Cu^{I}	$4s^{0.27}3d^{9.87}4p^{0.16}4d^{0.01}5p^{0.01}$	$4s^{0.27}3d^{9.87}4p^{0.17}4d^{0.01}5p^{0.01}$	$4s^{0.27}3d^{9.86}4p^{0.17}4d^{0.01}5p^{0.01}$
INT1	$4s^{0.34}3d^{9.54}4p^{0.27}4d^{0.01}5p^{0.01}$	$4s^{0.34}3d^{9.54}4p^{0.27}4d^{0.02}5p^{0.01}$	$4s^{0.35}3d^{9.54}4p^{0.26}4d^{0.02}5p^{0.01}$
TS1	$4s^{0.32}3d^{9.64}4p^{0.21}4d^{0.01}5p^{0.01}$	$4s^{0.35}3d^{9.39}4p^{0.27}4d^{0.01}5p^{0.01}$	$4s^{0.35}3d^{9.39}4p^{0.27}4d^{0.01}5p^{0.01}$
INT2	$4s^{0.37}3d^{9.31}4p^{0.30}4d^{0.01}5p^{0.01}$	$4s^{0.36}3d^{9.31}4p^{0.30}4d^{0.01}5p^{0.01}$	$4s^{0.37}3d^{9.31}4p^{0.29}4d^{0.01}5p^{0.01}$
TS2	$4s^{0.36}3d^{9.38}4p^{0.34}4d^{0.01}5p^{0.01}$	$4s^{0.35}3d^{9.38}4p^{0.34}4d^{0.01}5p^{0.01}$	$4s^{0.37}3d^{9.38}4p^{0.32}4d^{0.01}5p^{0.01}$
INT3	$4s^{0.32}3d^{9.34}4p^{0.26}4d^{0.01}5p^{0.01}$	$4s^{0.32}3d^{9.34}4p^{0.26}4d^{0.01}5p^{0.01}$	$4s^{0.33}3d^{9.34}4p^{0.24}4d^{0.01}5p^{0.01}$
INT4	$4s^{0.34}3d^{9.44}4p^{0.33}4d^{0.02}5p^{0.01}$	$4s^{0.34}3d^{9.45}4p^{0.32}4d^{0.02}5p^{0.01}$	$4s^{0.34}3d^{9.44}4p^{0.33}4d^{0.02}5p^{0.01}$
TS3	$4s^{0.31}3d^{9.69}4p^{0.21}4d^{0.02}5p^{0.01}$	$4s^{0.32}3d^{9.69}4p^{0.20}4d^{0.01}5p^{0.01}$	$4s^{0.32}3d^{9.70}4p^{0.18}4d^{0.01}5p^{0.01}$
INT5	$4s^{0.28}3d^{9.67}4p^{0.19}4d^{0.01}5p^{0.01}$	$4s^{0.28}3d^{9.66}4p^{0.21}4d^{0.01}5p^{0.01}$	$4s^{0.31}3d^{9.63}4p^{0.20}4d^{0.01}5p^{0.01}$
INT6	$4s^{0.38}3d^{9.31}4p^{0.26}5p^{0.01}$	$4s^{0.38}3d^{9.31}4p^{0.26}5p^{0.01}$	$4s^{0.39}3d^{9.31}4p^{0.25}5p^{0.01}$
INT7	$4s^{0.32}3d^{9.42}4p^{0.28}4d^{0.02}5p^{0.01}$	$4s^{0.31}3d^{9.42}4p^{0.28}4d^{0.02}5p^{0.01}$	$4s^{0.34}3d^{9.43}4p^{0.23}4d^{0.02}5p^{0.01}$
INT8	$4s^{0.38}3d^{9.36}4p^{0.23}4d^{0.01}5p^{0.01}$	$4s^{0.37}3d^{9.36}4p^{0.23}4d^{0.01}5p^{0.01}$	$4s^{0.37}3d^{9.36}4p^{0.24}4d^{0.01}5p^{0.01}$

Table S8. Natural electron configurations of Cu in intermediates and transition states at the 2AlH-Cu^{I} site of Cu-*cha*, Cu-*gme*, and Cu-*aft*.

species	*cha*	*gme*	*aft*
2AlH-Cu^{I}	$4s^{0.34}3d^{9.83}4p^{0.16}4d^{0.01}5p^{0.01}$	$4s^{0.33}3d^{9.83}4p^{0.16}4d^{0.01}5p^{0.01}$	$4s^{0.35}3d^{9.82}4p^{0.16}4d^{0.01}5p^{0.01}$
INT1	$4s^{0.33}3d^{9.54}4p^{0.29}4d^{0.02}5p^{0.01}$	$4s^{0.32}3d^{9.54}4p^{0.29}4d^{0.02}5p^{0.01}$	$4s^{0.33}3d^{9.53}4p^{0.29}4d^{0.02}5p^{0.01}$
TS1	$4s^{0.34}3d^{9.39}4p^{0.30}4d^{0.02}5p^{0.01}$	$4s^{0.34}3d^{9.38}4p^{0.29}4d^{0.02}5p^{0.01}$	$4s^{0.34}3d^{9.33}4p^{0.33}4d^{0.01}5p^{0.01}$
INT2	$4s^{0.35}3d^{9.34}4p^{0.39}4d^{0.01}5p^{0.01}$	$4s^{0.35}3d^{9.34}4p^{0.38}4d^{0.01}5p^{0.01}$	$4s^{0.36}3d^{9.34}4p^{0.38}4d^{0.01}5p^{0.01}$
TS2	$4s^{0.35}3d^{9.34}4p^{0.35}4d^{0.01}5p^{0.01}$	$4s^{0.34}3d^{9.34}4p^{0.35}4d^{0.02}5p^{0.01}$	$4s^{0.36}3d^{9.35}4p^{0.33}4d^{0.01}5p^{0.01}$
INT3	$4s^{0.30}3d^{9.32}4p^{0.29}4d^{0.01}5p^{0.01}$	$4s^{0.29}3d^{9.32}4p^{0.29}4d^{0.01}5p^{0.01}$	$4s^{0.29}3d^{9.32}4p^{0.30}4d^{0.01}5p^{0.01}$
INT4	$4s^{0.33}3d^{9.45}4p^{0.30}4d^{0.02}5p^{0.01}$	$4s^{0.33}3d^{9.45}4p^{0.30}4d^{0.02}5p^{0.01}$	$4s^{0.33}3d^{9.45}4p^{0.31}4d^{0.02}5p^{0.01}$
TS3	$4s^{0.27}3d^{9.65}4p^{0.27}4d^{0.025}p^{0.01}6s^{0.01}$	$4s^{0.31}3d^{9.69}4p^{0.20}4d^{0.01}5p^{0.01}$	$4s^{0.30}3d^{9.66}4p^{0.21}4d^{0.01}5p^{0.01}$
INT5	$4s^{0.26}3d^{9.66}4p^{0.25}4d^{0.02}5p^{0.01}$	$4s^{0.27}3d^{9.65}4p^{0.26}4d^{0.02}5p^{0.01}$	$4s^{0.25}3d^{9.66}4p^{0.25}4d^{0.02}5p^{0.01}$
INT6	$4s^{0.33}3d^{9.31}4p^{0.31}4d^{0.01}5p^{0.01}$	$4s^{0.34}3d^{9.29}4p^{0.31}4d^{0.01}5p^{0.01}$	$4s^{0.34}3d^{9.29}4p^{0.32}4d^{0.01}5p^{0.01}$
INT7	$4s^{0.34}3d^{9.29}4p^{0.32}4d^{0.01}5p^{0.01}$	$4s^{0.33}3d^{9.32}4p^{0.30}4d^{0.01}5p^{0.01}$	$4s^{0.33}3d^{9.28}4p^{0.32}4d^{0.01}5p^{0.01}$
INT8	$4s^{0.38}3d^{9.36}4p^{0.23}4d^{0.01}5p^{0.01}$	$4s^{0.29}3d^{9.30}4p^{0.22}4d^{0.01}5p^{0.01}$	$4s^{0.30}3d^{9.30}4p^{0.23}4d^{0.01}5p^{0.01}$

Table S9. Natural electron configurations of Cu in intermediates and transition states at the $[Cu^{II}(NH_3)_4]^{2+}$ site of Cu^{II}-2Al-*cha*, -*gme*, and *aft*.

species	*cha*	*gme*	*aft*
2Al-Cu^{II}	$4s^{0.37}3d^{9.34}4p^{0.28}4d^{0.03}$	$4s^{0.39}3d^{9.35}4p^{0.19}4d^{0.03}5p^{0.01}$	$4s^{0.37}3d^{9.34}4p^{0.27}4d^{0.02}$
INT1	$4s^{0.38}3d^{9.33}4p^{0.30}4d^{0.03}5p^{0.01}$	$4s^{0.38}3d^{9.34}4p^{0.26}4d^{0.03}5p^{0.01}$	$4s^{0.37}3d^{9.33}4p^{0.28}4d^{0.03}5p^{0.01}$
TS	$4s^{0.39}3d^{9.59}4p^{0.21}4d^{0.02}5p^{0.01}$	$4s^{0.37}3d^{9.65}4p^{0.19}4d^{0.02}5p^{0.01}$	$4s^{0.37}3d^{9.61}4p^{0.23}4d^{0.02}5p^{0.01}$
INT2	$4s^{0.51}3d^{9.74}4p^{0.16}4d^{0.02}5p^{0.01}$	$4s^{0.49}3d^{9.75}4p^{0.17}4d^{0.01}5p^{0.01}$	$4s^{0.48}3d^{9.76}4p^{0.17}4d^{0.02}5p^{0.01}$

Table S10. Natural electron configurations of Cu in intermediates and transition states at the 2Al-2Cu^{I} site of Cu-*cha*, Cu-*gme*, and Cu-*aft*.

species	*cha*	*gme*	*aft*
INT1	$4s^{0.50}3d^{9.77}4p^{0.13}4d^{0.02}5p^{0.01}$	$4s^{0.51}3d^{9.77}4p^{0.15}4d^{0.02}5p^{0.01}$	$4s^{0.52}3d^{9.78}4p^{0.13}4d^{0.02}5p^{0.01}$
	$4s^{0.55}3d^{9.77}4p^{0.13}4d^{0.01}5p^{0.01}$	$4s^{0.53}3d^{9.77}4p^{0.18}4d^{0.02}5p^{0.01}$	$4s^{0.50}3d^{9.78}4p^{0.13}4d^{0.02}5p^{0.01}$
INT2	$4s^{0.36}3d^{9.56}4p^{0.22}4d^{0.02}5p^{0.01}$	$4s^{0.39}3d^{9.57}4p^{0.18}4d^{0.02}5p^{0.01}$	$4s^{0.33}3d^{9.53}4p^{0.21}4d^{0.02}5p^{0.01}$
	$4s^{0.29}3d^{9.58}4p^{0.24}4d^{0.02}5p^{0.01}$	$4s^{0.40}3d^{9.60}4p^{0.23}4d^{0.02}5p^{0.01}$	$4s^{0.31}3d^{9.50}4p^{0.21}4d^{0.02}5p^{0.01}$
INT3	$4s^{0.30}3d^{9.48}4p^{0.31}4d^{0.02}$	$4s^{0.32}3d^{9.48}4p^{0.19}4d^{0.02}5p^{0.01}$	$4s^{0.30}3d^{9.48}4p^{0.30}4d^{0.02}$
	$4s^{0.30}3d^{9.48}4p^{0.31}4d^{0.02}$	$4s^{0.32}3d^{9.48}4p^{0.20}4d^{0.02}5p^{0.01}$	$4s^{0.30}3d^{9.48}4p^{0.30}4d^{0.02}$
TS	$4s^{0.34}3d^{9.35}4p^{0.37}4d^{0.02}$	$4s^{0.35}3d^{9.37}4p^{0.24}4d^{0.02}5p^{0.01}$	$4s^{0.34}3d^{9.35}4p^{0.37}4d^{0.02}$
	$4s^{0.34}3d^{9.35}4p^{0.37}4d^{0.02}$	$4s^{0.35}3d^{9.37}4p^{0.23}4d^{0.02}5p^{0.01}$	$4s^{0.34}3d^{9.35}4p^{0.37}4d^{0.02}$
INT4	$4s^{0.39}3d^{9.24}4p^{0.41}4d^{0.01}$	$4s^{0.39}3d^{9.24}4p^{0.37}4d^{0.01}5p^{0.01}$	$4s^{0.37}3d^{9.23}4p^{0.43}4d^{0.01}$
	$4s^{0.39}3d^{9.24}4p^{0.40}4d^{0.01}$	$4s^{0.38}3d^{9.24}4p^{0.37}4d^{0.01}5p^{0.01}$	$4s^{0.37}3d^{9.23}4p^{0.43}4d^{0.01}$

XVII. NPA charge of Cu in Cu-*cha*, Cu-*gme*, and Cu-*aft*.

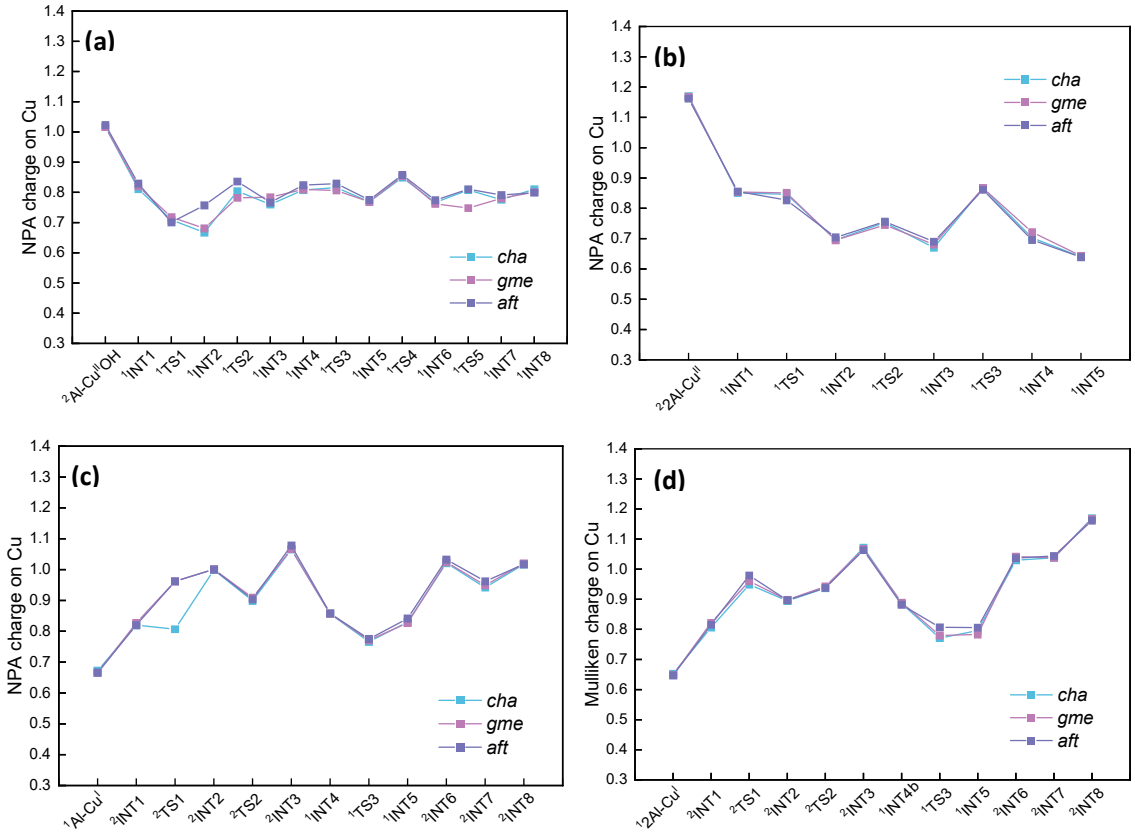

Figure S11. Natural population analysis (NPA) charge on the Cu ions of intermediates and transition states during the reduction (a, b) and oxidation (c, d) processes. (a, c) show the processes on the Al site, and (b, d) show the processes on the 2Al site. The superscript numbers along the horizontal axes represent the spin multiplicity of the ground state.

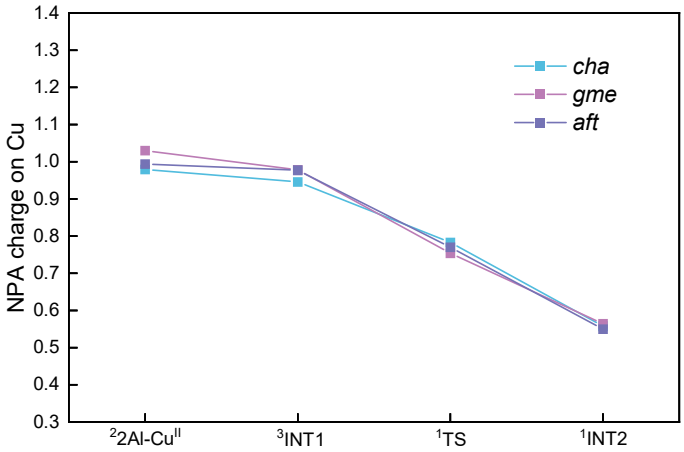

Figure S12. NPA charge on the Cu ions of intermediates and transition states during reduction at the $[Cu^{II}(NH_3)_4]^{2+}$ site of Cu^{II}-2Al-*cha*, -*gme*, and *aft*. The superscript numbers along the horizontal axes represent the spin multiplicity of the ground state.

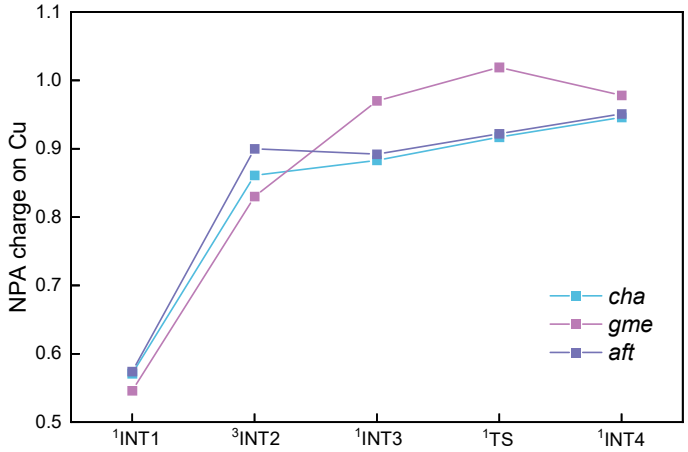

Figure S13. NPA charge on the Cu ions of intermediates and transition states during reduction at the 2Al-2Cu^{I} site of Cu-*cha*, Cu-*gme*, and Cu-*aft*. The superscript numbers along the horizontal axes represent the spin multiplicity of the ground state.